ChemComm

Accepted Manuscript

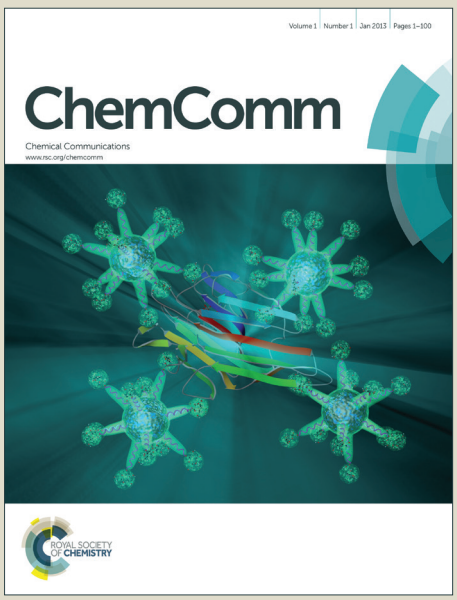

ROYAL SOCIETY OF CHEMISTRY

www.rsc.org/chemcomm

Cite this: DOI: 10.1039/c0xx00000x

www.rsc.org/xxxxxx

ARTICLE TYPE

Post modification of MOF derived carbon via g-C_3N_4 entrapment for efficient metal-free oxygen reduction reaction

Sekar Pandiaraj†, Harshitha Barike Aiyappa†, Rahul Banerjee* and Sreekumar Kurungot*

Received (in XXX, XXX) Xth XXXXXXXXX 20XX, Accepted Xth XXXXXXXXX 20XX
DOI: 10.1039/b000000x

High surface area carbon with a nitrogen content of 7.0 % is derived from MOF via *in situ* g-C_3N_4 formation. The material shows excellent ORR activity with an onset potential of 0.035 V (*vs.* Hg/HgO) in alkaline medium apart from high durability and strong disinclination towards methanol crossover.

Over the past decade, high surface area-hetero atom doped carbon materials have been in the limelight due to their colossal applications in energy fields, such as fuel cells, lithium ion batteries, super capacitors, and dye sensitized solar cells (DSSC) etc[1]. Among the various methods available, the frontrunners include chemical vapour deposition (CVD), template assisted carbon synthesis, nitrogen plasma treatment, thermal annealing with NH_3 apart from pyrolysis of carbon with nitrogen precursors such as pyridine, cyanamide, etc[2]. These heteroatom doped materials such as N doped graphene, CNTs etc. have been exclusively tried in fuel cell systems[2c], considering their additional CO tolerance and fuel selectivity under the operating conditions. The doping is found to alter the electron density of carbon, thereby generating the active sites needed for ORR[3]. However, these methods suffer from acute disadvantages viz., harsh acid post-treatment, use of toxic precursors, specially designed equipments, rigorous handling conditions, etc[4]. Furthermore, most importantly, these methods do not allow precise control on the extent of nitrogen doping. This could be mainly due to the high temperature annealing which compels easy escape of the nitrogen precursors from the reactant zone, thereby resulting in inefficient doping and eventual decrease in the number of active sites[5]. Thus, a lookout for a novel approach to increase the ORR kinetics along with the sidewise maintenance of surface area, so as to enable faster mass transfer apart from creation of more active sites, turns out to be a grand challenge in the development of new generation electrocatalysts.[6]

On account of their self-sacrificial nature, high carbon content and inherent porosity, MOFs have been recently used to derive highly porous carbon structures thereby ruling out the need for any additional carbon sources[7]. They could be directly used for anchoring the incoming hetero atoms[8]. Among the N precursors, by virtue of its high N content, graphitic carbon nitride (g-C_3N_4) has been used as an effective catalyst for numerous reactions such as photocatalytic hydrogen generation, water splitting[9] etc. However, the pristine g-C_3N_4 material is found to exhibit limited activity due to its low electrical conductivity and minimum surface area. Henceforth, one of the ways to overcome this limitation could be the incorporation of g-C_3N_4 into a highly mesoporous and conductive carbon backbone thereby creating a much better and closer requisite for ORR[10]

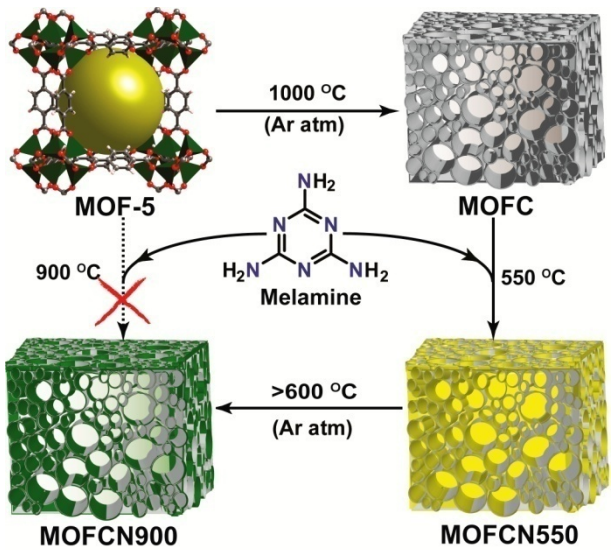

Scheme 1. Construction of N-doped porous carbon formed g-C_3N_4 on melamine impregnation into the pores of carbonized MOF-5 followed by carbonization at higher temperature (> 600 °C).

In the present work, we report the designing of an ORR electrocatalyst consisting of carbonized g-C_3N_4 and nanoporous carbon. Herein, we attempt to effectively utilize the macro porosity of carbon as a nitrogen reservoir through initial plugging of g-C_3N_4 units via *in situ* polymerization of melamine. Moreover, the defects arising from micropores present in the carbon skeleton could be expected to render anchoring sites for the incoming N atoms. On further heating, g-C_3N_4, decomposes releasing its nitrogen content which eventually gets doped into the nearby carbon skeleton[12]. In the current work, two synthetic routes were attempted and MOF-5 was chosen owing to its high surface area and carbon content[11]. In the first route, porous carbon obtained on direct pyrolysis of MOF-5 and melamine were ground together (mass ratio 1:5), dispersed in ethanol solution followed by stirring at room temperature for 12 h. The resulting material was separated by solvent evaporation and then heated in an Ar flow at 550 °C for 3h. The as synthesized MOFCN550 composite was then carbonized at 800, 900 and 1000 °C each in an Ar atmosphere for 3 h. The samples were denoted as MOFCN800, MOFCN900 and MOFCN1000 respectively. In the second route, as regularly followed in literature, direct impregnation of N source into the MOF crystal

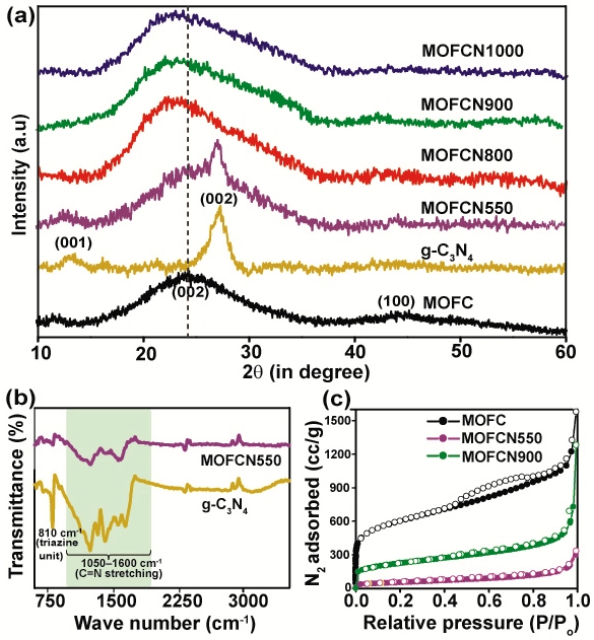

Fig. 1. a) The PXRD pattern obtained for the samples heated at different temperatures. b) IR spectra of MOFCN550 and pristine g-C_3N_4carbons. c) N_2 adsorption study of MOFC, MOFCN550 and 900.

matrix was carried out. The MOF-5 crystals and melamine precursors were directly dispersed in ethanol and stirred overnight. The solid mass was pyrolysed at 900 °C in an Ar flow and the resulting sample is denoted as MOF5-CN. The detailed procedure is described in the supplementary part (Part S1).The PXRD pattern of MOF-5 derived carbon (MOFC) exhibits peaks at ~25 and ~44° corresponding to the diffractions from the (002) and (100) graphitic carbon planes respectively, which suggest the presence of long range ordering in the carbon matrix (Fig 1a). The absence of ZnO peaks confirms the purity of the resulting mesoporous carbons. In case of g-C_3N_4, a strong diffraction peak at 27° corresponding to the interlayer stacking of the aromatic melamine units has been observed. The PXRD of MOFCN550 consists of the peaks corresponding to both g-C_3N_4 and MOFC which further confirms the polymerization of melamine and *in situ* formation of g-C_3N_4 at 550 °C. The samples heated at higher temperatures, shows a blue shift in the (002) peak position (from ~25 to ~24.2) which suggests a possible intercalation of N atoms inside the carbon matrix thereby introducing N doping in the end carbon.[12] The MOF5-CN shows carbon peaks at values 26°and 44°, similar to other carbons. (Fig. S1).

The IR spectrum of the composite prepared at 550 °C confirms the presence of g-C_3N_4 (bands at 810 and 1050–1600 cm^{-1} correspond to the breathing mode of triazine units and C=N stretching respectively) inside the MOF derived carbon, as can be seen in case of pristine g-C_3N_4 (Fig. 1b). On g-C_3N_4 incorporation, the surface area of the MOFC composite dramatically decreases from 2184 to 276 m^2/g, indicating the possible plugging of the carbon pores with g-C_3N_4. In case of MOFCN900, the surface area further increased to 765 m^2/g following the decomposition of g-C_3N_4 at 900 °C (Fig. 1 c). From Raman spectra, of all the carbons, MOFCN800 shows higher I_D/I_G ratio of 1.28, due to the highest N content followed by MOFCN900 (1.22) and MOFCN1000 (1.13) (Fig. S3). The XPS

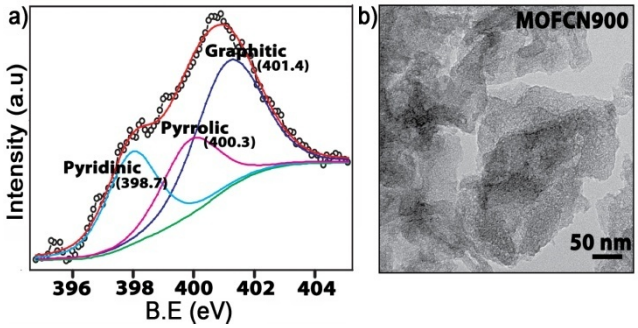

spectra and EDX analysis also reveal a

Fig. 2. a) The deconvoluted XPS N1s spectra and b) TEM image of MOFCN900.

decrease in the total N content with increase in the pyrolysis temperature. Of all, MOFCN800 shows highest N content (8.26%) followed by MOFCN900 (7.0 %) and MOFCN1000 (4.74%).The deconvoluted XPS spectra shows the presence of three types of nitrogens, pyridinic (398.7 eV), graphitic (401.4 eV) and pyrrolic (400.3 eV) respectively. It was observed that on rise in temperature from 800 to 900 °C, conversion of pyridinic-N into graphitic-N was being favored[11] (Fig. S4 and Table 1 SI). Among all the samples, MOFCN900 shows the highest graphitic N content (~47 %). Conversely, the EDX analysis of MOF5-CN reveals the presence of very low N content of 1.2% along with Zn impurities which hints the possible presence of metal residues in trace limits (Fig S6).This apparently hints the ineffective doping due to the rapid decomposition of g-C_3N_4 at higher temperature. Further, it could be understood that the decrease in the I_D/I_G ratio and N content in case of MOFCN900 and MOFCN1000 could be a result of poor doping with rise in temperature. The TEM image of MOFC shows the presence of micropores in the carbon matrix. MOFCN550 indicates the presence of g-C_3N_4 particles with slate like structure of the carbon matrix (Fig. S2). On the other hand, MOFCN900 shows the presence of microporous sheet very much similar to that of MOFC which further indicates the transition of g-C_3N_4 into porous N doped carbon without any apparent evidence of the plugged g-C_3N_4 (Fig 1c). The TGA profile of MOFCN550 reveals a weight loss above 550 ºC which indicates the decomposition of the plugged g-C_3N_4 (Fig. S7).

Cyclic voltammetry (CV) and rotating disc electrode (RDE) measurements were performed using a three-electrode system with 0.1 M KOH as electrolyte, Hg/HgO as reference and Pt wire as counter electrodes (Fig. 3a and S8).The linear sweep voltammogram (LSV) studies reveal the superiority of MOF derived carbon over the commercial Vulcan carbon in terms of its higher positive onset potential and limiting current density (Fig. S9). This could be a result of the former's high surface area and intrinsic porosity which leads to improved mass transfer and diffusion of electrolytes towards the active sites, thereby resulting in better ORR activity. On further functionalization, a remarkable favored shift in the onset potential could be observed, due to the generation of more number of active sites. Of all the composites prepared, MOFCN900 shows the highest electrochemical performance with a well defined cathodic peak at -0.09 V. However, on further rise in temperature, a decrease in the catalytic performance is observed. This ascertains the reduction in the number of active sites with decrease in the N content in the

system. The LSV of MOFCN800 shows an onset potential at

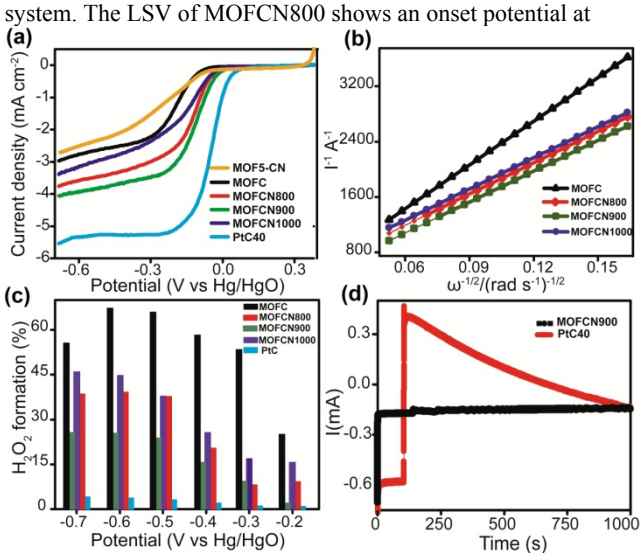

Fig 3. a) Combined steady state polarization plots under O_2 saturated conditions in 0.1M KOH at a scan rate of 10 mV/s with electrode rotation of 1600 rpm b) K-L plots derived from the polarization studies c) Bar graphs corresponding to the H_2O_2% formed using RRDE d) Chrono amperometric responses on CH_3OH addition at 150 s.

0.0V and a current density of 3.74 mA/cm^2, which is comparatively higher than that of the as such MOF derived carbon. On increasing the temperature to 900 ºC (as in case of MOFCN900), the onset potential is found to have shifted towards 0.035 V along with an improved current density of 4.2 mA/cm^2, although the N content decreases to about 7 %. It thus fares well in comparison to PtC40 with an over potential of just 65 mV. This enhancement in the onset potential obtained for MOFCN900 catalyst is higher compared to the 50-150 mV difference in the onset potential reported for most of the hetero atom doped carbon materials. (Table 4, SI). However, the sample MOF5-CN shows an onset at -0.095V, which is lower than MOFCN900 (Table 2, SI). This may be due to the presence of Zn impurities in MOF5-CN, which minimizes the nitrogen doping. This decreases the number of active sites, thereby reducing its catalytic activity. The reaction kinetics of all the samples was further studied by rotating ring disc electrode (RRDE) technique (Fig. 3c, Fig. S10). Of all, MOFCN900 showed an e^- transfer number of 3.12 with a peroxide yield of only 15 % at -0.4 V, indicating a greater contribution from the desired 4e^- pathway (derived using K-L plot, Fig. 3b) which hints a favorable shift in the ORR kinetics on nitrogen doping. Thus, as evident from its influence on the electrochemical performance of the current materials of interest, as well from the previous literature, it could be ascertained that graphitic-N forms the major active site for ORR. From these results, it can be observed that the amount of N and right combination of the types of N (graphitic and pyridinic) play a crucial role in ORR. The accelerated durability test (ADT) was conducted by cycling the potential between -0.15 to 0.15 V for 1000 cycles. The linear sweep voltammograms clearly shows that PtC40 suffers a negative potential shift of 40 mV *vs.* Hg/HgO, whereas, the observed potential degradation for the in-house metal-free catalyst is only 30 mV (Fig. S11). It therefore reveals the superior electrochemical stability of the in-house catalyst. Further, the chronoamperometric study proves that unlike the Pt catalyst, MOFCN900 does not show a change in current upon addition of CH_3OH (Fig. 2d). It thus substantiates the higher tolerance of the in-house catalyst towards fuel crossover and CO poisoning.

In conclusion, new electrocatalysts have been designed by simple impregnation of melamine into MOF-5 derived mesoporous carbon thereby enriching the nitrogen content to 7.0 - 8.3% besides maintaining high surface area. Among all, MOFCN900 shows enhanced ORR activity comparable to that of the commercial Pt catalyst. This can be attributed to the synergetic effect between the highly ordered mesoporous carbon, which improves the mass transfer along with improved diffusion of electrolyte towards the active sites, and g-C_3N_4 intermediate which helps in the generation of the desired N-doped active sites (graphitic and pyridinic in this case). In addition to the enhanced ORR activity, the catalyst is found to possess high fuel selectivity and superior durability. This route thereby opens a new pathway for the design and development of metal-free electrodes as fuel cell cathodes. Such N-doped carbon composites have enormous potential applications in various renewable energy fields' viz. fuel cells, solar cells, supercapacitors and so on.

Acknowledgements:

K.S and S.P acknowledge DST, India, for the financial support through the project (No. SR/S1/PC-05/2011). H.B.A is thankful to UGC, India, for the research fellowship.

Notes and references

***Physical and Materials Chemistry Division, CSIR-National Chemical Laboratory**, Dr. Homi Bhabha Road, Pune 411008, India; Tel: +912025902566; E-mail: k.sreekumar@ncl.res. r.banerjee@ncl.res.in.*

† S.P and **H.B.A** contributed equally to this work.

† Electronic Supplementary Information (ESI) available: Experimental procedures, XPS study, TGA plots, electrochemical study viz., ADT and additional supporting data.See DOI: 10.1039/b000000x/

(1) Z. Chen, D. Higgins, A. Yu, L. Zhang, and J. Zhang, *Energy Environ. Sci*, 2011, **4**, 3167.

(2) a) L.Qu, Y.Liu, J. B. Baek, and L. Dai, *ACS Nano* 2010, **4,** 1321.b) P. Pachfule, V. M. Dhavale, S. Kandambeth, K. Sreekumar, and R. Banerjee, *Chem. Eur. J.* 2013, **19**, 974. c) K.Gong, F. Du, Z. Xia, M.Dustock, and L.Dai, *Science* 2009, **323**, 760.

(3) Y.Wang, Y.Shao, D. Matson, J.Li, and Y.Lin, *ACS Nano* 2010, **4,**1790.

(4) A. Olejniczak, M. Lezanska, J. Wloch,A. Kucinskaa and J. P. Lukaszewicza , *J. Mater. Chem. A*, 2013, **1**, 8961.

(5) a)X. Li, H. Wang, J. T. Robinson, H. Sanchez, G. Diankov, and H. Dai, *J. Am. Chem. Soc.*, 2009, **131,** 15939.

(6) a) H. Chang, S.H. Joo and C. Pak, *J. Mater. Chem.*, 2007, **17**, 3078.

(7) a) H.L. Jiang, B.Liu, Y.Q. Lan, K. Kuratani, T. Akita, H. Shioyama, F. Zong, and Q. Xu, *J. Am. Chem. Soc.*, 2011, **133** , 11854. b)H. B. Aiyappa, P. Pachfule, R.Banerjee, and K.Sreekumar, *Cryst. Growth Des*, 2013, **13** , 4195.

(8) T.Palaniselvam, B. P. Biswal, R. Banerjee, and K. Sreekumar , *Chem. Eur. J.* 2013, **19**, 9335.

(9) a) Y. J .Zhang, T. Mori, and J. H. Ye, *Sci. Adv. Mater,* 2012, **4**, 282. b) X. Wang, K. Maeda, A. Thomas, K. Takanabe, G. Xin, J. M. Carlsson, K. Domen, and M. Antonietti *Nat. Mater,* 2009, **8,**76.

(10) S. M. Lyth, Y. Nabae, S. Moriya, S. Kuroki, M. Kakimoto, J. Ozaki, and S. Miyata, *J. Phys. Chem. C, 2009,* **113,** 20148. b) Y. Zhang, T. Mori, L. Niu, and J. Y. *Energy Environ. Sci*, 2011, **4**, 4517.

(11) a) N. L. Rosi, J. Eckert, M. Eddaoudi, D. T. Vodak, J. Kim, M. O'Keeffe, O. M. Yaghi, *Science*, 2003, **300**, 1127.

(12) a) K. Parvez, S.Yang, Y. Hernandez, A. Winter, A. Turchanin, X. Feng, and K. Mullen, *ACS Nano*, 2012, **6**, 9541.